



HAL
open science

Laser Path Optimization For Additive Manufacturing

M Boissier, G. Allaire, Christophe Tournier

► **To cite this version:**

M Boissier, G. Allaire, Christophe Tournier. Laser Path Optimization For Additive Manufacturing. The World Congress of Structural and Multidisciplinary Optimization, May 2019, Beijing, China. hal-02310434

HAL Id: hal-02310434

<https://hal.science/hal-02310434v1>

Submitted on 10 Oct 2019

HAL is a multi-disciplinary open access archive for the deposit and dissemination of scientific research documents, whether they are published or not. The documents may come from teaching and research institutions in France or abroad, or from public or private research centers.

L'archive ouverte pluridisciplinaire **HAL**, est destinée au dépôt et à la diffusion de documents scientifiques de niveau recherche, publiés ou non, émanant des établissements d'enseignement et de recherche français ou étrangers, des laboratoires publics ou privés.

LASER PATH OPTIMIZATION FOR ADDITIVE MANUFACTURING

M. Boissier^{1,2*}, G. Allaire², C. Tournier³

¹CMAP, Ecole Polytechnique, CNRS UMR7641, 91128, Palaiseau, France

* Corresponding author: mathilde.boissier@polytechnique.edu

²LURPA, ENS Cachan, Université Paris-Saclay, 94325, Cachan, France

Abstract

Additive Manufacturing (AM) through a Laser Powder Bed Fusion (LPBF) process consists in building objects layer by layer, by depositing energy in metallic powder with a laser along a chosen path. Despite huge advantages, such as the freedom in the design, this manufacturing process causes defects in the resulting object. Choosing the laser path is of high significance, since it is tightly related to both the manufacturing speed and the temperature distribution in each layer. The design of the laser path is often based on optimizing parameters of existing patterns and combining them. A different approach is proposed here. Without presupposing any specific pattern, our method is based on shape optimization theory and a descent algorithm is drafted to adapt the path to the manufacturing requirements.

Keywords: *Shape Optimization, Additive Manufacturing, Selective Laser Melting, Laser Powder Bed Fusion, Laser Path*

1. Introduction

The LPBF process consists in building objects layer by layer, according to the following scheme: metallic powder is regularly distributed and then a laser, moving along a planned trajectory, brings energy to melt the metal. The cooling brings the solidification and post-processes are finally applied. This method presents many advantages: complex designs can be manufactured and an adjusted producing is facilitated, getting free from the constraints of mass-production [3]. However, some very strict rules can't be forgotten. Indeed, some supports have to be anticipated depending on the manufacturing angles, post-processes are mandatory to empty the object from the powder trapped in, to increase the item's features or to remove residual stresses created by the process. These mechanical drawbacks are the focal point of this work. Indeed, the energy deposition by the laser induces more than a simple melting of the powder. It also creates expansion, residual constraints, surface tension in the melting pool [1,4,5,8,9]. Adapting the laser path is a track to improve the final properties of the solid. Among the many existing strategies [5,9], most of them are based on a few amount of patterns only. The objective of this work is to develop strategies without presupposing any pattern, using shape optimization tools, focusing mainly on reducing the thermic expansion. Section 2 first establishes the physical model, and then, Section 3 sets the representation of the trajectory chosen as well as the optimization tools. Numerical results are shown in Section 4 before mentioning, in Section 5, the perspectives of this work.

2. Model presentation of the LPBF process

2.1 The model's scales

To build a layer, the powder is first melted creating a liquid state, the melting pool, and involving a gas phase. Then, from the cooling, this melted metal solidifies. Thus, many phenomena, related to physics or mechanics are involved and an accurate model is required (Fig. 1). Two different scales are set apart [4,8]:

- a microscopic scale, taking into accounts the melting pool and thus the liquid and gaseous states. In this model, the characteristics of the material depend non linearly on the temperature. Moreover, an advanced study of the fluid mechanics phenomena is realized. The evaporation of material and the surface tension, including normal and tangential stresses, are considered, and the defaults induced by the process are well highlighted. However, the huge number of variables, equations, as well as their non linearity make the use of optimization algorithms at this scale computationally too expensive.

- a macroscopic scale, "forgetting" the melting pool and thus roughly keeping only two states: powder and solid. The

change of states is considered as an abrupt change in the material properties and only three thermal phenomena are taken into accounts: conduction, convection and radiation. The interaction between the heat source and the powder is simplified. This approach does not allow for an accurate quantification of the different phenomena. However, it is enough to highlight the thermal expansion and the appearance of residual stresses during the manufacturing, both of them implying important defaults in the object and resulting into early damage and fatigue. The computational cost of this scale is from far lower than the microscopic scale, allowing for optimization algorithms to be used.

2.2 Presentation of the model considered for path optimization

We aim in this article at optimizing the laser path in order to build the object while controlling the thermal expansion. A macroscopic scale would thus provide the information required without leading to costly resolutions of the physics [1,4,8]. Since the thermal stress can be expressed as Eq.1:

$$\sigma_{th} = C(T - T_{init})I_d, \quad (1)$$

with C depending on the thermal expansion coefficient and on the elastic properties of the material, T_{init} the initial temperature and d the dimension of the problem, the thermal expansion can be controlled in a first step by constraining the maximal temperature in the item during the manufacturing. Due to the unbalanced effects between conduction on the one hand and convection and radiation on the other hand, once enough layers have been built, convection and radiation are ignored. Thus, the model equations come down to heat equation with conduction within the domain D , absorption of energy where the laser beam is applied (on the top layer) and Dirichlet boundary condition on the bottom layer, where the temperature is maintained to a chosen temperature T_{init} (Fig. 2). In this model, only powder and solid are considered. The physical characteristics such that the density ρ , the specific heat c , the conduction λ , are considered as in Eq.2 [1]:

$$A(t, x) = A_{solid}\chi_{solid}(t, x) + A_{powder}(1 - \chi_{solid}(t, x)), \quad (2)$$

with χ_{solid} the characteristic function of the solid. Moreover, it is assumed that the working domain D is surrounded by an adiabatic material (the working domain is in fact surrounded by powder, which conductivity is very low. The real value of this conductivity is thus considered in the working domain D and taken equal to 0 outside). The source is considered to be a Gaussian beam [4,8], matching Eq.3, with P_{tot} the source power, A the absorption coefficient, r_b the beam radius and $r(X, t)$ the distance to the source's center. To simplify this formulation, an effective power P and a coefficient δ are introduced.

$$q(t, X) = \frac{AP_{tot}}{\pi r_b^2} \exp\left(-A \frac{r(X, t)^2}{r_b^2}\right) = P \exp(-\delta r(X, t)^2), \quad (3)$$

The resultant equation is Eq.4:

$$\begin{cases} \rho(t, X)c(t, X)\partial_t T(t, X) - \nabla_X \cdot (\lambda(t, X)\nabla_X T(t, X)) = 0 & \text{in } D \times (0, t_F), \\ \lambda(t, X)\nabla_n T(t, X) = q(t, X) & \text{on } \partial D_{top} \times (0, t_F), \\ \lambda(t, X)\nabla_n T(t, X) = 0 & \text{on } \partial D_{side} \times (0, t_F), \\ T(t, X) = T_{init}(X) & \text{on } \partial D_{bottom} \times (0, t_F), \\ T(0, X) = T_{init}(X) & \text{in } D. \end{cases} \quad (4)$$

Two huge simplifications are then applied to this model, to ease the computation and allow for a setting of the path optimization with shape optimization methods: the representation is first reduced to two dimensions and the computations are run in the layer plane, and then, only the steady case is considered. It is clear that the resulting model does not correspond to the reality but they still provide some intuition about the optimized trajectories and allow for a validation of the method. Removing these two simplifications is part of the future work perspectives (see Section 5).

In the LPBF process, the (Oz)-axis is the building direction, and each layer is in the (Oxy)-surface. The working domain can thus be considered as $D = \Sigma \times (-L, 0)$, with Σ the layer plane. The two dimensional model is drawn from the three dimensional one by focusing on only one layer. Whereas we had $X = (x, y, z)$ in Eq.4, we now consider $X' = (x, y)$. T source term, previously applied on the top layer, is now a volumic source of heat in the surface Σ . Let's forget about the

physical parameters and set $\Delta' = \partial_x^2 + \partial_y^2$ such that $\Delta T = \Delta' T + \partial_z^2$. An integration along the (Oz)-axis, between $(-L)$ and 0, gives, assuming that $\Delta' T$ and $\partial_t T$ don't depend on z :

$$\int_{-L}^0 \rho c \partial_t T + \lambda \Delta T dz = \int_{-L}^0 \rho c \partial_t T + \lambda \Delta' T dz + \int_{-L}^0 \partial_z^2 T dz = \rho c L \partial_t T + L \lambda \Delta' T + \lambda [\partial_z T]_{-L}^0, \quad (5)$$

Assume now that, to model the conduction through the (Oz)-axis, there is a Fourier boundary condition, with coefficient β , on the surface characterized by $\{z = -L\}$. Since β is related to the conduction in the (Oz)-axis, it could be taken as $\beta = \frac{\lambda_{solid}}{\Delta Z}$, with ΔZ a characteristic length. The model chosen for the heat equation in two dimensions is given by Eq.5:

$$\begin{cases} \rho(t, X') c(t, X') \partial_t T(t, X') - \nabla_{X'} \cdot (\lambda(t, X') \nabla_{X'} T(t, X')) + \frac{\lambda_{solid}}{\Delta Z L} T(t, X') = \frac{1}{L} q(t, X') & \text{in } \Sigma \times (0, t_F), \\ \lambda(t, X') \nabla_n T(t, X') = 0 & \text{on } \partial \Sigma \times (0, t_F), \\ T(0, X') = T_{init}(X') & \text{in } \Sigma. \end{cases} \quad (6)$$

In the steady model, the source is no longer moving. Instead, we decide to apply the laser on the whole trajectory, introducing a steady source Q ($Q = P_Q \chi_\Gamma$, with P_Q a linear power divided by a characteristic length and χ_Γ the Dirac mass for the path Γ). This model includes the mathematical difficulties brought by the optimization process. It is thus a very useful first step to set the optimization problem. However, it does not represent the physics correctly and must be kept as a ‘‘toy model’’. All the coefficients will be arbitrarily fixed and won't match any real parameter. Choosing the conductivity $\lambda(X')$ to be the powder's conductivity, the resulting equation is Eq.5:

$$\begin{cases} -\nabla_{X'} \cdot (\lambda_{powder} \nabla_{X'} \tilde{T}(X')) + \frac{\lambda_{solid}}{\Delta Z L} \tilde{T}(X') = \frac{1}{L} Q(X') = \frac{P_Q}{L} \chi_\Gamma(X') & \text{in } \Sigma, \\ \nabla_n \tilde{T}(X') = 0 & \text{on } \partial \Sigma, \\ T(X') = \tilde{T}(X') + T_{init} & \text{in } \Sigma. \end{cases} \quad (7)$$

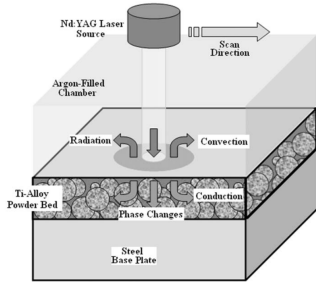


Figure 1. LPBF process

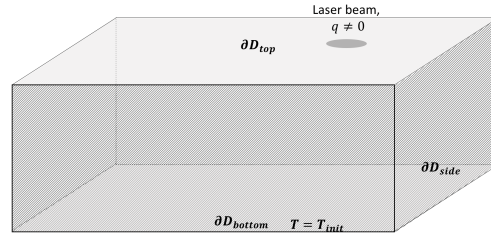


Figure 2. Three dimensional simplified model

3. Shape optimization through front tracking methods

3.1 Shape optimization

Shape differentiation's theory, introduced by Hadamard, and widely developed since, can be used for optimization, and consists in deforming a reference domain Ω_0 in the direction of a vector field θ [1,2,7]. The admissible shapes are then

$$\Omega = (I_d + \theta)(\Omega_0) = \{x + \theta(x) \text{ such that } x \in \Omega_0\}, \quad (8)$$

and the definition of shape differentiability is the following:

Definition: Let Ω_0 an open bounded domain. A function $J: \Omega \rightarrow \mathbb{R}$ is differentiable at Ω_0 with respect to the shape if the application $\theta \rightarrow J((I_d + \theta)(\Omega_0))$ is Fréchet-differentiable at 0 on $C^1(\mathbb{R}^d, \mathbb{R}^d)$ and

$$J((I_d + \theta)(\Omega_0)) = J(\Omega_0) + DJ(\Omega_0)(\theta) + o(\theta), \quad (9)$$

with $DJ(\Omega_0)(\theta)$ linear form on $C^1(\mathbb{R}^d, \mathbb{R}^d)$ and $\lim_{\theta \rightarrow 0} \frac{|o(\theta)|}{\|\theta\|} = 0$.

The following theorem yields the general form of the derivative for a two dimensional curve:

Proposition: Let Γ_0 be a regular oriented curve in \mathbb{R}^2 and set A and B its end points. The tangent, τ , is defined with respect to the orientation of the curve and the normal, n , so that at each point, (τ, n) is an orthonormal basis of \mathbb{R}^2 .

Let $f \in W^{2,1}(\mathbb{R}^2)$ and J such that $J(\Gamma) = \int_{\Gamma} f(s) ds$. Then, J is differentiable at Γ_0 and, for all $\theta \in C^1(\mathbb{R}^2, \mathbb{R}^2)$, with κ the curve's curvature,

$$J'(\Gamma_0)(\theta) = \int_{\Gamma_0} [\nabla_n f + \kappa f](s) \theta(s) \cdot n(s) ds + f(B) \theta(B) \cdot \tau(B) - f(A) \theta(A) \cdot \tau(A). \quad (10)$$

3.2 Trajectory model

We wish to adapt shape optimization theory to the design of laser beam paths. The problem of representing a curve or contour in a domain \tilde{D} comes into many different fields (shape optimization, fluid mechanics, computer vision, ...) and has been widely studied [11,12]. Among the many approaches, we highlight the main ones: Lagrangian methods, in which the mesh is adapted to the contour at each iteration, Eulerian methods, aimed at keeping the same computational mesh at all time (from which the Marker and Cell (MAC), Volume of Fluid and level set methods are drawn) and mixed approach. Front tracking methods have been chosen here, with the manipulation of two different meshes: one for the working domain, that will be called "mesh" in the following, and one for the contour, referred to as "discretized path". Equations are designed to adapt the values from the mesh to the discretized path [12]. In the present work, the path is discretized using segments and is thus represented by a broken line. The shape derivative computed and regularized [1,2,7] in the continuous context can be discretized and each node of the discretized path is then advected. To keep a correct description, the resulting line is re-discretized: each segment's size of the discretized path is controlled (Fig.3). This re-discretization consists in removing points in case of an excessively small segment and adding points if the distance overtakes a fixed one. In this study, points are added equidistantly but other means could be used (Legendre methods to increase the accuracy of the approximation of functions on the domain for example). This technique displays different benefits. There is no need to re-mesh the whole domain at each iteration and on the other hand, it drives the fact that the trajectory is oriented and very easy to handle, allowing complex shapes. Loops for example, would be very hard to be dealt with using level set or MAC methods whereas they turn up to be simple with front tracking ones. Eventually, the topology is fully controlled (Fig.4).

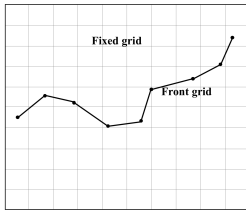


Figure 3. Curve advection

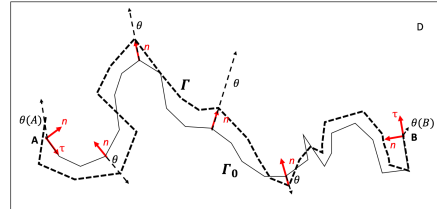


Figure 4. Front tracking method

4. Numerical results under steadiness hypothesis

4.1 Problem description

Two constraints have been considered. First of all, the aim of the LPBF process is to build an object and thus, the whole item must have changed from powder to solid during the manufacturing. In the steady context, this results in the following constraint, with T_ϕ the phase change temperature and $\forall X \in \mathbb{R}, X^+ = \max(X, 0)$:

$$C_\phi(\Gamma) = \int_{\Sigma} \left[(T_\phi - T(x))^+ \right]^2 dx. \quad (11)$$

The second constraint aims at controlling the thermal expansion and thus affects the maximum temperature. A maximal admissible temperature T_M is defined and the second constraint is:

$$C_M(\Gamma) = \int_{\Sigma} [(T(x) - T_M)^+]^2 dx. \quad (12)$$

Finally, the length of the manifold Γ is optimized under the two previous constraints and the state equation Eq.6.

4.2 Numerical results

Some numerical tests have been run to validate the method. We consider here a working domain $D = [-10cm, 10cm] \times [-10cm, 10cm]$. The domain is discretized with a triangular mesh having 3200 elements (the

characteristic length of an element is 0.07). The accuracy of the discretized path is defined by the distance ΔP between two nodes and we have $0.02 \leq \Delta P \leq 0.06$. The source term is a P0 function. Indeed, for each element of the mesh, the length of the path crossing the triangle has been computed and scaled. This P0 function is multiplied by a power, P. In this simulation, the conductivity has been chosen as [1] $\lambda_{solid} = 15W.m^{-1}.K^{-1}$, $\lambda_{powder} = 0.25W.m^{-1}.K^{-1}$ and the phase change temperature $T_\phi = 1700 K$, which correspond to the value for a maraging steel. As for the other values, they have been arbitrarily chosen so that the optimization is possible, and we set $\Delta Z = 1 m$, $L = 10 cm$, $P_Q = 700 W.m^{-2}$, $T_{init} = 500K$. The maximum temperature is $T_M = 2000 K$. The finite element computations are run with Freefem software [6] and an Augmented Lagrangian algorithm is chosen. The line evolution is shown on Fig.5 whereas Fig.6 presents the evolution of the length and constraints with respect to the iterations.

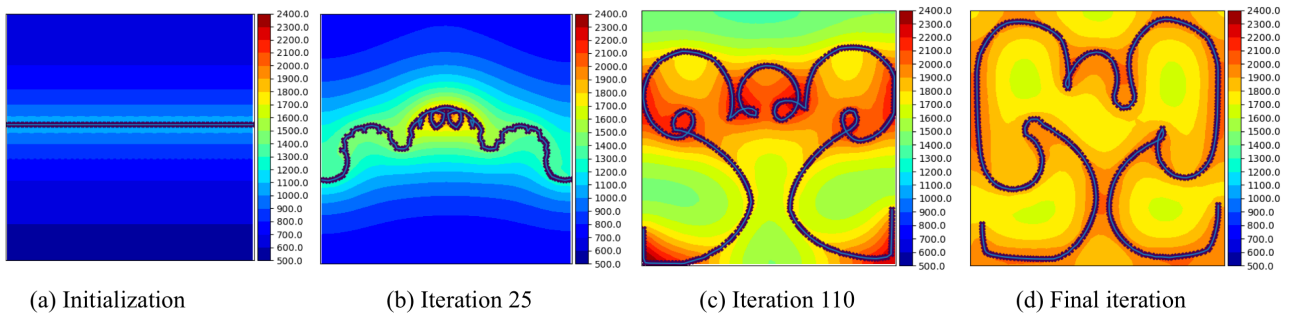


Figure 5. Evolution of the line and temperatures (K)

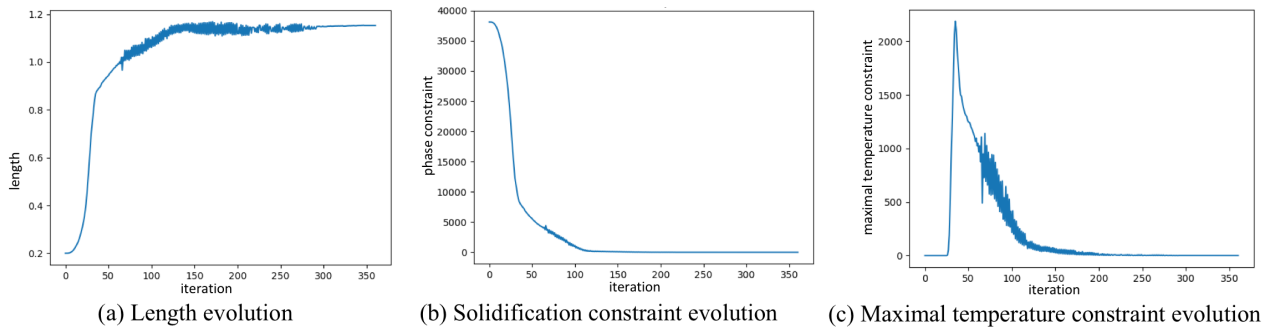


Figure 6. Evolution of the length and constraints

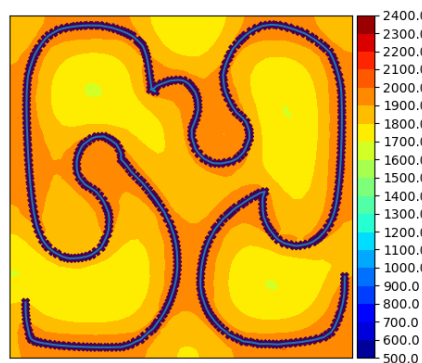


Figure 7. Final path, after a second optimization

At the end of this first optimization, the constraints are not fully satisfied. The algorithm is run again, changing slightly the regularization of the shape derivative, being initialized by the final iteration shown in Fig.5. The final path is shown by Fig.7. The constraints are then satisfied ($C_\phi < 0.001$ and $C_M < 0.001$) and the length is optimized, validating the method. It is important to remark that the result presented by Fig. 5 is a local optimum of the problem. Thus, choosing an

other initialization may lead to a different solution path.

5. Conclusion

This work allows for a validation of the use of shape optimization tools to optimize the laser path in the steady case. This illustrates the interest of this method for path optimization and calls for further investigations. A first option consists in a deeper study of the steady case. Indeed, it allows for a very fast computation of the heat and induces a very easy optimization process. The design of the path could be improved in this model by understanding better the dependence of the results from the optimization parameters, by adding an optimization variable such as the source power. One could also think of getting free from the two dimensional assumption, getting a 3D model and optimizing the path on many layers, thus collecting information on the dependence in the vertical axis. Finally, more constraints such as a control of the temperature gradient within the solid would improve the result, bringing them closer to the physical reality.

Another generalization is of course to consider the unsteady model. The optimization process will get more complex but the interpretation of the results will be immediate. These results will be some good basis to develop more intuition and design new patterns that could then be implemented in the industry.

Acknowledgments

The authors would like to thank the SOFIA project, funding this work.

References

1. G. Allaire, L. Jakabčín, Taking into accounts residual stresses in topology optimizationf structures built by additive manufacturing, *Maths. Models Methods Appl. Sci.* 28(12) :2313-2366, 2018.
2. G. Allaire, F. Jouve, A-M. Toader, Structural optimization using sensitivity analysis and a level-set method, *J. Comput. Phys.* 194(1) :363-393, 2004.
3. A. Bernard, C. Barlier, *Fabrication additive, du prototypage rapide à l'impression 3D*, Dunod, 2015.
4. T. DebRoy, H.L. Wei, J.S. Zuback, et al., Additive manufacturing of metallic components - Process, structure and properties, *Progress in Materials Science*, 92:122-224, 2018.
5. D. Ding, Z. Pan, D. Cuiuri, H. Li, S. Van Duin, *Advanced Design for Additive Manufacturing, 3D Slicing and 2D Path Planning*, *New Trends in 3D Printing*, InTech, 2016.
6. F. Hecht, New development in FreeFem++, *Journal of Numerical Mathematics*, 252-265, 2012.
7. A. Henrot, M. Pierre, *Shape variation and optimization. A geometrical analysis*, EMS Tracts in Mathematics, 28., Zürich, 2018.
8. M. Megahed, H-W. Mindt, N. N'Dri, H. Duan, O. Desmaison, Metal additive-manufacturing process and residual stress modeling, *Integrating Materials and Manufacturing Innovation*, 5(4):1-33, 2016.
9. S. Mohanty, J-H. Hattel, Cellular scanning strategies for selective laser melting : generating reliable, optimized scanning paths and processing parameters, *Proceedings of SPIE, Laser 3D Manufacturing II 9353:93530U*, 2015.
10. J. Nocedal, S.J. Wright, *Numerical Optimization*, Springer science+ Business Media, 2006.
11. S. Osher, R. Fedkiw, *Level set methods and dynamic implicit surfaces*, *Applied Mathematical Sciences*, 153. Springer-Verlag, New-York, 2003.
12. G. Tryggvason et al., A front-tracking method for the computations of multiphase flow, *J. Comput. Phys.* 169(2) :708-759, 2001.